Chapter 8
Design and Analysis of One-Dimensional Photonic Crystal Biosensor Device for Identification of Cancerous Cells

Abinash Panda and Puspa Devi Pukhrambam

Abstract The present chapter highlights one-dimensional photonic crystal (1D PhC) and its vital applications. The remarkable scientific progress in PhC has been able to draw the attention of researchers for novel bio-sensing applications. With the advancement in technology, different defect-based PhCs have been successfully fabricated with extensive analysis of propagation characteristics and tested for various sensing applications like blood, gas, salinity, DNA, alcohol, liquid, food, hormones, enzymes, cells, urine, glucose, chemicals, etc. The transfer matrix method is the most suitable method to study the spectral characteristics of 1D PhC structure. The sensing principle is based on the study of alteration in the resonant mode wavelength according to the modification in the analyte refractive index. This chapter deals with the study of defect-based 1D PhC cancer cells sensor, where TMM is employed to detect basal, cervical, and breast cancer cells. In order to enhance the sensitivity, a thin graphene layer is deposited at the side wall of the defect layer. A complete optimization of geometrical parameters has been performed to envisage high performance. The 3D colormap plot is studied to clearly show the variation in the properties of the defect mode with change in the incident angle. Moreover, signal-to-noise ratio, Q-factor, resolution, and figure of merit of the sensor are measured meticulously. The noteworthy sensing performance can open an avenue to effectively detect the cancer cells in the early stage.

8.1 Introduction

Most of the technological innovation have brought up by deeply perceiving the nature. There are numerous examples which validate the existence of periodic nature

A. Panda (✉) · P. D. Pukhrambam
Department of Electronics and Communication Engineering, National Institute of Technology Silchar, Silchar, Assam 788010, India
e-mail: abinashpanda087@gmail.com

P. D. Pukhrambam
e-mail: puspa.devi@ece.nits.ac.in

G. Dutta and A. Biswas (eds.), *Next Generation Smart Nano-Bio-Devices*,
Smart Innovation, Systems and Technologies 322,
https://doi.org/10.1007/978-981-19-7107-5_8

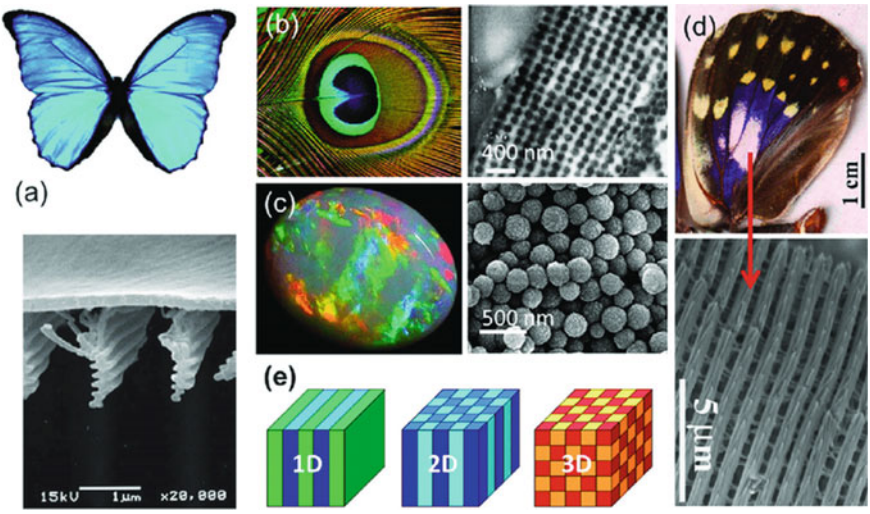

Fig. 8.1 Natural photonic crystals **a** morph butterfly, **b** multi-colored peacock feather, **c** opal gemstone, **d** wing of Sasakia Charonda with their microscopic images, **e** 1D/2D/3D PhCs

of variations in nature. For example, wings of butterflies, opal of the bracelet, feathers of birds, and barbules of colorful birds contain a systematic periodic arrangements, which resemble with the property of photonic crystals [1–3]. The color changes with respect to the angle of observation, which is primarily owing to the interaction between the light and the above-mentioned material's natural design. Figure 8.1 demonstrates some nature-based multilayer effects.

The study on periodic multilayer structures by E. Yablonvitch and S. John in the early 1987 is considered as the flagship research on photonics, which ignited the minds of the researchers to explore different applications using photonics principle [4, 5]. In their work, the authors revealed the effect of periodicity in two dimensions and three dimensions. As far as research on photonic crystal is concerned, it can be realized in 1D, 2D, and 3D forms. Among these, 3D PhCs are facing fabrication feasibility issues, and still research is going on to find an effective fabrication technique to produce low-loss 3D PhCs [6, 7]. On the other hand, 2D PhCs can be successfully fabricated by etching technique resulting in triangular, square, and honeycomb structures. The 2D PhCs can be designed in the form of slab, which can be organized in two ways: arrangement of dielectric materials with air as the background and arrangement of holes on a dielectric slab [8–10]. Defect-based PhCs have brought the revolution in the photonics research community. The defects can be created by omitting a series of air holes or by altering the properties of air holes along a particular shape in the PhC, which makes it behaves as a photonic crystal waveguide (PCW) [11–13]. The light signals fall within the PBG can be effectively guided and trapped in PCW, which enables the manipulation of electromagnetic

waves in the nano-structure. Nonetheless, several efforts have been given by scientists and researchers to mimic 2D and 3D PhCs, but 1D PhCs are the utmost explored structures and investigated from theoretical to experimental aspects due to their fabrication feasibility, high compatibility, and broad application domain [14–16]. The 1D PhCs are blessed with an elegant characteristics called as photonic band gap (PBG), which appears owing to the periodical arrangement of different dielectric materials along the stacking direction [17]. The PBG reflects that wavelength band which is restricted to propagate along the multilayer structure. The PBG characteristic of the 1D PhC has a significant effect in envision of many novel applications such as laser applications, sensing applications, filter, optical mirror, polarizer, communication applications, biomedical applications [18–20]. PhC must be structurally altered to produce a resonant mode in the spectral characteristics in order to be used as a biosensor. The finest technique to create such a resonant mode is to insert a defect in the design [21]. If the input wavelength and the defect mode wavelength matches each other, a discrete spike is formed in the spectral characteristics. The light (photons) are strongly localized near the defect layer [22]. A slight change in the surrounding refractive index leads to a significant modification in the location of the defect mode. Till now, 1D PhCs are widely used for a variety of purposes [23–26]. Moreover, 1D PhCs are highly reliable pertaining to temperature fluctuations, offer fast operation, and possess higher lifetime compared to the high-dimensional PhCs.

In the last decade, researchers have explored numerous novel 2D materials, which be integrated with photonic devices to improve the performance. Graphene has come up as a promising material for the design of various optical devices and therefore evolved as a center of attraction of researchers worldwide [27, 28]. A. Geim and K. Novoselov first introduced graphene as a 2D material, for which they received the prestigious Nobel Prize in the year 2010 [29, 30]. Graphene possesses a unique lattice configuration and is considered as a novel material due to its outstanding electronics properties. Graphene has hexagonally arranged lattice structure of sp2 hybridization having noteworthy electronic properties. Most importantly, graphene has a higher conductivity of 10^6 s/m and a very low resistivity of 10^{-6} Ω·cm, which makes it convenient to work in a broad applications domain compared to the conventional materials [31]. Moreover, graphene demonstrates zero bandgap properties and excellent carrier mobility. Even though, the approximate thickness of graphene is only 0.34 nm, but still it shows a remarkable absorption property [32]. It has been experimentally observed that a monolayer of graphene can absorb 2.3% of light in a wide wavelength band. Owing to its high absorption property, graphene shows distinguished reflectance for TE and TM modes under total internal reflection, which is very sensitive toward a small deviation in the RI of the contacting surface [33]. Due to the aforementioned properties, graphene has successfully entered the photonics industry to realize different electromagnetics applications. The properties like flexibility, durability, robustness, high conductivity, excellent mobility, etc. make graphene a right candidate for design of photonic devices [34–36]. Notably, the conductivity of graphene can be adjusted by controlling the chemical potential across the graphene sheet. So by suitably controlling the chemical potential across the graphene sheet, the optical properties of the integrated graphene photonic devices can

be varied according to the user requirement. From the energy band transition point of view, two types of interactions are noticed between graphene and light signal, namely inter-band transition and in-band transition. The inter-band transition is mainly seen in visible to NIR wavelength range, whereas the in-band transition is observed in the far-infrared wavelength regime. In case of in-band transition, graphene behaves as a free electron which is capable of exciting the surface. Nevertheless, a monolayer of graphene bestows high light absorption, but it shows a poor absorption of only 2.3% as material, which demands a more deep research to boost the interaction between graphene and electromagnetic signal.

Since the last two decades, 1D PhCs are dominating in the field of designing biosensors. A 1D PhC sensor is proposed by W. Nouman et al. for detection of brain lesions within the refractive index range of 1.3333 to 1.4833 and achieved an excellent sensitivity of 3080.8 nm.RIU^{-1} [37]. Z. Zaky et al. reported a Tamm plasmon structure to detect various gases. Ag plays a vital role in generating the plasmonic modes at the interface between the metal and 1D PhC [38]. A thorough analysis is carried out on the characteristics of the defect modes, where it is seen that the cavity resonance tends to decrease with an escalation in the RI of the targeted gases [39]. A. Ahemad explored a Psi-based photonic crystal including a metal layer and investigated Tamm plasmon polariton (TPP) resonant modes for sensing liquid analytes. The authors studied the shifting nature of the defect mode by infiltrating the cavity with liquids of different refractive index [40]. A. H. Aly manipulated TMM to examine the transmission spectrum in a defect 1D PhC for sensing the creatinine concentrations in blood [41]. A. Panda et al. studied the absorption spectrum and transmission spectrum in both symmetric and asymmetric 1D PhC structure to detect various viruses present in the drinking water, which find a suitable application in rural area [17]. A hemoglobin sensor is realized by M. Abadla and his team to sense a wide concentrations of hemoglobin. After optimizing numerous structure parameters, they attained a sensitivity of 167 nm per RIU [42]. A glucose sensor is designed using defect-based 1D PhC through the analysis of reflectance characteristics [43]. A steady and low-cost sensor is reported by Elsayed et al. [44], to sense various types of biodiesels. The bandgap properties of a 1D PhC comprising a single layer of graphene sandwiched between the dielectric materials is inspected by J. Fu et al. [45]. A graphene-based 1D PhC is investigated by Fan et al., where the authors explored the dependence of optical properties of graphene on its chemical potential [46]. By varying the chemical potential, the authors measured the change in the defect mode frequency. A novel protein sensor is investigated on the ground of 1D PhC. Although the authors used the optimized parameters, they found a sensitivity of only 170 nm per RIU, which is not up to the mark [47].

Cancer, the leading reason of fatality worldwide, has evolved as a precarious diseases. As per the information of IARC, around 19.3 million population around the globe are contrived by the cancer, and nearly 10 million fatalities have occurred in the year 2020 [48]. The primary reason behind the growth of cancer cells in human body is the interaction between the genetic factors of the body with different external agents like physical carcinogens, chemical carcinogens (tobacco, aflatoxin), and biological carcinogens (bacteria, viruses) [49]. Due to this effect, the cells grow in uncontrolled

manner by absorbing relatively more protein and nutrients from the body [50]. The main point of concern is that till date there is no fully guaranteed treatment of cancer in medical science. Probably, the single approach to combat the situation is the early detection of this diseases. So, a label-free and point of care cancer testing device is indispensable to effectively fight with cancer. In the last decade, researchers have greatly relied on photonics technologies to successfully detect different cancer cells with high accuracy and less time. A cancer cell sensor is proposed by Bijalwan et al., which is consisted of alternating layers of SiO_2 and TiO_2. The authors used TMM technique to achieve a sensitivity of 73 nm/RIU [51]. A. Aly et al. optimized the geometrical parameters of a 1D PhC and tested the spectral characteristics of the structure by filling different cancer cells in the defect layer. The authors are settled with a sensitivity of 2200 nm/RIU [52]. The transmission spectrum of a defected photonic crystal is analyzed in detail by Ramanujam and his team, where a very low sensitivity of 43 nm/RIU is achieved, which is very low [53]. A point defect-based 2D photonic crystal waveguide is studied for detection of different types of cancer cells. In their work, the authors rely on the electric filed analysis in the defect region and measured the reflected wavelength, which differentiated the normal cells from the cancer cells [54]. N. Ayyanar et al. investigated a dual core photonic crystal fiber to detect various cancer cells like cervical, basal cells, etc. [55]. Sani et al. studied the bandgap characteristics in a 2D photonic crystal to differentiate cancer cells from the normal cells [56]. Jabin et al. attempted to integrate a metal layer in the core of the photonic crystal fiber and studied the plasmonic behavior of the device. Further, the authors tested their device to distinguish cells infected with cancer cells in a broad wavelength band of visible to NIR regime [57].

8.2 Theoretical Formulation

This chapter explores a 1D PhC, which is realized as a regular periodic arrangements of MgF_2 and ZnSe. A cavity/defect layer is formed at the center of the arrangement. A monolayer of graphene sheet is sandwiched between the defect layer and the dielectric layer. The alignment of the whole structural arrangement is $(MgF_2/ZnSe)^N$/graphene/defect/graphene/$(MgF_2/ZnSe)^N$, which is represented in Fig. 8.2. The thickness of the layer MgF_2, ZnSe, and graphene is represented as d_A, d_B, and d_G, respectively. The cavity is loaded with different cancer cells. A 589 nm light, produced from a laser source, is made to strike the proposed structure normally along the x–z plane.

The constituent material RI plays a significant part in finding the spectral response of the entire configuration. The RI of MgF_2 and ZnSe can be measured with the help of Sellemier equations [58, 59],

$$n_{\mathrm{ZnSe}}^2 = 4 + \frac{1.90\lambda^2}{\lambda^2 - 0.113} \tag{8.1}$$

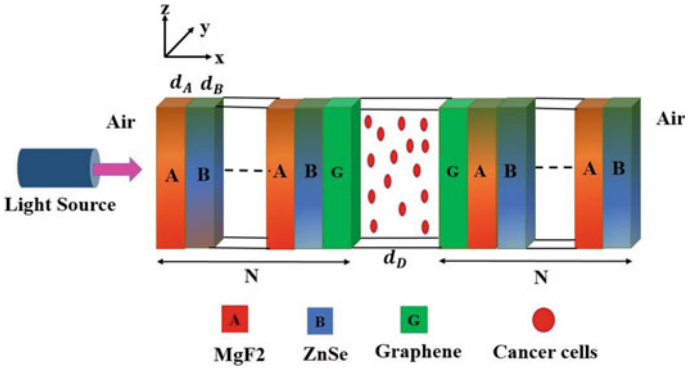

Fig. 8.2 Schematic of the proposed sensor

$$n^2_{\mathrm{MgF2}} = 1 + \frac{0.48755\lambda^2}{\lambda^2 - 0.04338^2} + \frac{0.39875\lambda^2}{\lambda^2 - 0.09461^2} + \frac{2.31203\lambda^2}{\lambda^2 - 23.7936^2} \tag{8.2}$$

The dielectric permittivity of graphene is stated as [60],

$$\varepsilon_G = \begin{bmatrix} \varepsilon_{\mathrm{Gt}} & 0 & 0 \\ 0 & \varepsilon_{\mathrm{Gt}} & 0 \\ 0 & 0 & \varepsilon_{G\downarrow} \end{bmatrix} \tag{8.3}$$

The terms $\varepsilon_{\mathrm{Gt}}$ and $\varepsilon_{G\downarrow}$ denote the normal and tangential component of permittivity, respectively. $\varepsilon_{G\downarrow} = 1$, and $\varepsilon_{\mathrm{Gt}}$ is expressed as below,

$$\varepsilon_{\mathrm{Gt}} = 1 + i\frac{\sigma(\omega)}{\varepsilon_0 \omega d_G} \tag{8.4}$$

where ω signifies the angular frequency, d_G denotes the graphene thickness, and ε_0 is the permittivity of air. The surface conductivity (σ_ω) regulates the physical properties of graphene. The transfer matrix representation of the graphene layer takes the form, $M_G = \begin{bmatrix} 1 & 0 \\ -\sigma_\omega & 1 \end{bmatrix}$, where σ_ω can be mathematically expressed by Kubo formula [61] as written below,

$$\sigma_\omega = \sigma_\omega^{\mathrm{intra}} + \sigma_\omega^{\mathrm{inter}} \tag{8.5}$$

$$\sigma_\omega^{\mathrm{intra}} = \left(\frac{ie^2}{8\pi\hbar}\right)\left[\frac{16K_BT}{\hbar\omega}\log\left(2\cosh\left(\frac{\mu_c}{2K_BT}\right)\right)\right] \tag{8.6}$$

$$\sigma_\omega^{\mathrm{inter}} = \left(\frac{e^2}{4\hbar}\right)\left[H(\hbar\omega - 2\mu) - \frac{i}{2\pi} \times \left(\log\left(\frac{(\hbar\omega + 2\mu)^2}{\hbar\omega - 2\mu^2 + (2K_BT)^2}\right)\right)\right] \tag{8.7}$$

where, H denotes the Heaviside step function, K_B represents the Boltzmann constant, ω be the angular frequency, e is the electron charge, μ_c represents the chemical potential, and T is the temperature in kelvin scale.The field components can be written as,

$$\begin{pmatrix} E_p \\ H_p \end{pmatrix} = \begin{pmatrix} \exp(-\mathrm{i}q_p y) & \exp(iq_p y) \\ -n_s \exp(-\mathrm{i}q_p y) & n_s \exp(iq_p y) \end{pmatrix} \begin{pmatrix} A_p \\ B_p \end{pmatrix} \tag{8.8}$$

All the terms in Eq. (8.8) are defined in Ref. [41]. The field components between the adjacent layers of p and $p+1$ are stated as [17],

$$\begin{pmatrix} E_p \\ H_p \end{pmatrix} = \frac{1}{2} \begin{pmatrix} [\exp(iq_p\alpha_p) + \exp(-iq_p\alpha_p)] & \left(-\frac{1}{\gamma_p}\right)[\exp(iq_p\alpha_p) - \exp(-iq_p\alpha_p)] \\ -\gamma_p[\exp(iq_p\alpha_p) - \exp(-iq_p\alpha_p)] & [\exp(iq_p\alpha_p) + \exp(-iq_p\alpha_p)] \end{pmatrix} \times \begin{pmatrix} E_{p+1} \\ H_{p+1} \end{pmatrix} \tag{8.9}$$

where $\alpha_p = d_p \cos\theta_p$. Here, d_p and θ_p signify the thickness and incident angle, respectively. The widely accepted transfer matrix method (TMM) is manipulated for studying the spectral characteristics of the projected 1D PhC. The TMM describes the discrete layer p in matrix form, which can be stated as [17],

$$M_p = \begin{bmatrix} \cos\sigma_p & \left(-\frac{i}{\emptyset_p}\right)\sin\sigma_p \\ -i\emptyset_p \sin\sigma_p & \cos\sigma_p \end{bmatrix} \tag{8.10}$$

For TE mode, σ_p and $\emptyset_p$. are defined as,

$$\sigma_p = \frac{2\pi}{\lambda} d_p n_p \cos\theta_p \text{ and } \emptyset_p = n_p \cos\theta_p \tag{8.11}$$

The TMM of the entire structure can be calculated by multiplying the characteristics matrix of the each layer and can be written as [44],

$$M = (M_A M_B)^N M_{\mathrm{MXene}} M_D M_{\mathrm{MXene}} (M_A M_B)^N = \begin{bmatrix} M(1,1) & M(1,2) \\ M(2,1) & M(2,2) \end{bmatrix} \tag{8.12}$$

The transmission and reflection coefficients are stated as [43],

$$t = \frac{2\gamma_0}{(M(1,1) + M(1,2)\gamma_1)\gamma_0 + (M(2,1) + M(2,2)\gamma_s)} \tag{8.5.13}$$

$$r = \frac{(M(1,1) + M(1,2)\gamma_s)\gamma_0 - (M(2,1) + M(2,2)\gamma_s)}{(M(1,1) + M(1,2)\gamma_s)\gamma_0 + (M(2,1) + M(2,2)\gamma_s)} \tag{8.5.14}$$

where $\gamma_0 = \sqrt{\mu_0/\varepsilon_0} n_0 \cos\theta_0$ and $\gamma_s = \sqrt{\mu_0/\varepsilon_0} n_s \cos\theta_s$.

Lastly, transmittance (T) and reflectance (R) are numerically expressed as [17],

$$T = \frac{\gamma_s}{\gamma_0} \left| t^2 \right| \text{ and } R = |r|^2 \tag{8.15}$$

Absorbance can be computed as [42],

$$A = 1 - T - R \tag{8.16}$$

8.3 Results Analysis

In this chapter, different cancer cells like breast, basal, and cervical cells are considered, which are received from different body parts in liquid form. The sensing principle relies on the contrast in index value of the normal and infected cell. The experimental refractive index (RI) data collected from references [62, 63] are enumerated in Table 8.1.

The geometrical parameters of the designed structure are properly optimized to accomplish a sharp and high-intensity resonant mode inside the bandgap. We consider $d_{\mathrm{MgF2}} = 150\,\mathrm{nm}$, $d_B = 150\,\mathrm{nm}$, $d_G = 0.34\,\mathrm{nm}$, $\varepsilon_{\mathrm{MgF2}} = 1.90$, $\varepsilon_B = 6.8$, and $N = 5$. TMM is employed to analyze the transmission spectrum by changing the width of the cavity region, angle of incidence, and chemical potential across the graphene sheet. Initially, an attempt is taken to show the effect of graphene on the transmission characteristics. As shown in Fig. 8.3a, by including the graphene layer, the intensity of the resonance mode increases, which is suitable for sensing purpose. With the presence of graphene, the overall transfer matrix is updated, which is the reason behind the red-shifting of defect mode wavelength. Figure 8.3b demonstrates the study of the defect mode characteristics with reference to different period (N) of the photonic crystal. As, it can be seen, at $N = 5$, maximum intensity with lowest FWHM is obtained, which is considered as the most apposite result. For higher values of N, the FWHM is relatively higher and therefore not suitable from sensor design point of view.

By setting $D = 500$ nm, $\theta_{\mathrm{in}} = 0°$, $\mu_c = 0.2\,\mathrm{eV}$, we simulated the proposed multilayer structure in COMSOL Multiphysics software to study the electric field

Table 8.1 Cell's refractive index

Cell type	RI
Normal	1.35
Basal	1.38
Cervical	1.392
Breast	1.399

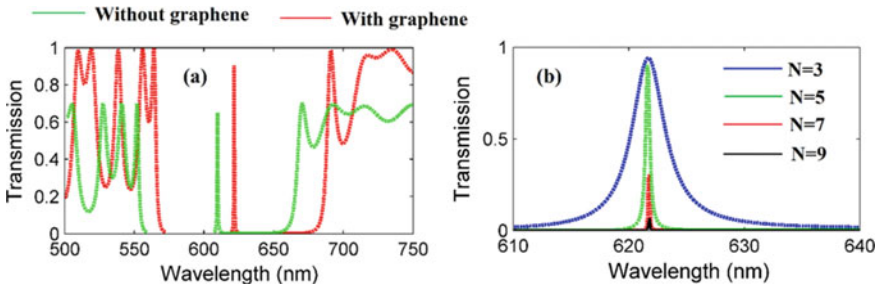

Fig. 8.3 **a** Effect of graphene layer on the transmittance spectrum, **b** variation in the period of the crystal

propagation in the structure, which is represented in Fig. 8.4. Owing to the presence of graphene layer, most of the light is confined inside the defect layer thereby increasing the interaction between light and infiltrated cancer cells. An electric field intensity in the order of 10^3 V/m is observed inside the cavity layer and gradually decays to both the sides of the defect layer.

For understanding the nature of variation of the defect mode, a colormap plot has been studied in Fig. 8.5, which shows the change in the transmission characteristics with respect to the wavelength and incident angle. In this figure, the high-intensity defect mode can be clearly seen inside the bandgap.

The transmission spectrum is examined for numerous selected cells at varied cavity layer thicknesses, which is depicted in Fig. 8.6. A substantial shift in the resonant mode is observed from normal to cancer type cells. In particular, the resonant wavelength (λ_{res}) experiences a red-shift as we infiltrate the cavity layer from the normal cells to the cancerous cells. This shifting nature closely follows the standing wave condition [26]. At $d_D = 500$ nm, the λ_{res} is moved from 621.6 to 633.8 nm

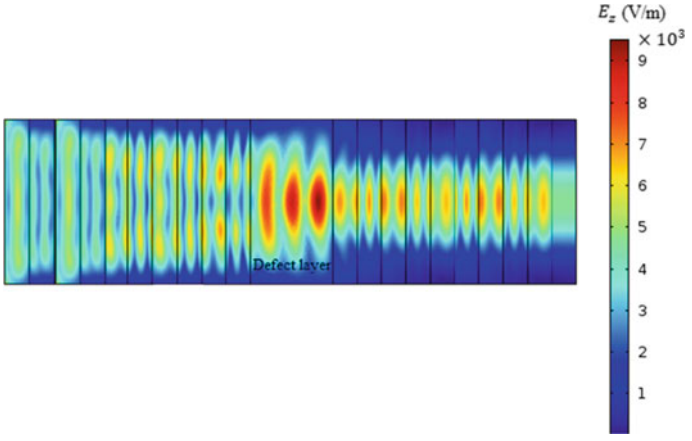

Fig. 8.4 Electric field distribution in the proposed structure

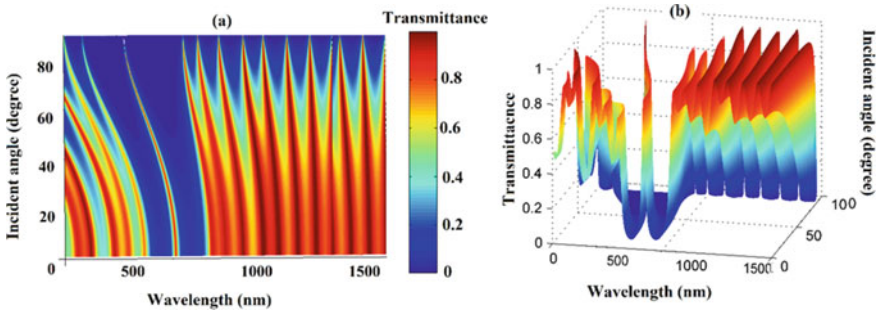

Fig. 8.5 Study of the colormap plot

as the cell type is changed from normal to breast cancerous cell. At $d_D = 600$ nm, the λ_{res} experiences a total shift from 612.3 to 625.5 nm, at $d_D = 700$ nm, the λ_{res} undertakes a total shift from 604.8 to 618.8 nm. Similarly, at $d_D = 800$ nm, the λ_{res} experiences a total shift from 898.8 to 613.3 nm.

Afterward, incident angle is varied, and the change in the defect mode properties is studied as demonstrated in Fig. 8.7. By increasing incident angle (θ_{in}) from 25° to 50°, the defect mode position experiences a blue-shift. This analysis is carried out at all the considered values of d_D. The blue-shifting nature of the defect mode is in accordance with the Bragg condition [26].

A thorough analysis on transmission spectrum is performed at $d_D = 500$ nm and $\theta_{in} = 0°$, by varying the number of graphene layers (L) from $L = 1$ to $L = 4$, which

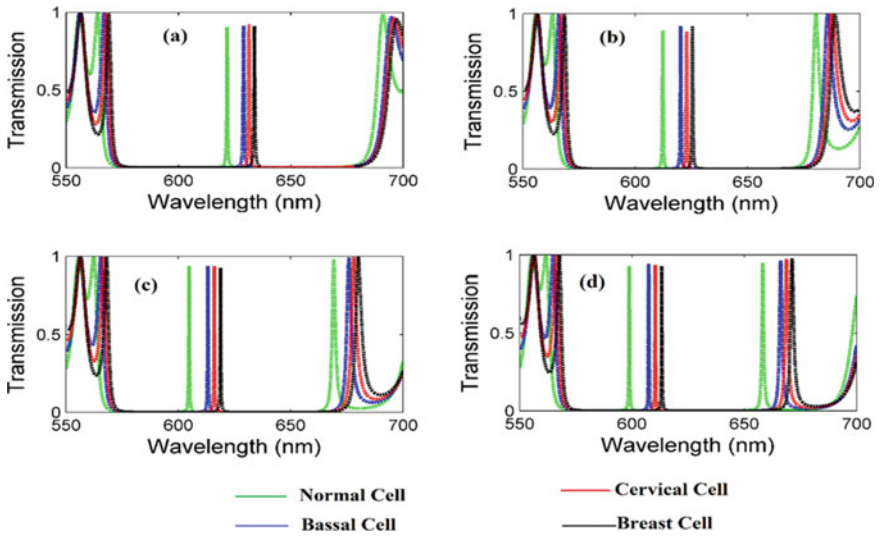

Fig. 8.6 Transmittance spectrum of different cells under normal incidence at **a** $d_D = 500$ nm, **b** $d_D = 600$ nm, **c** $d_D = 700$ nm, **d** $d_D = 800$ nm

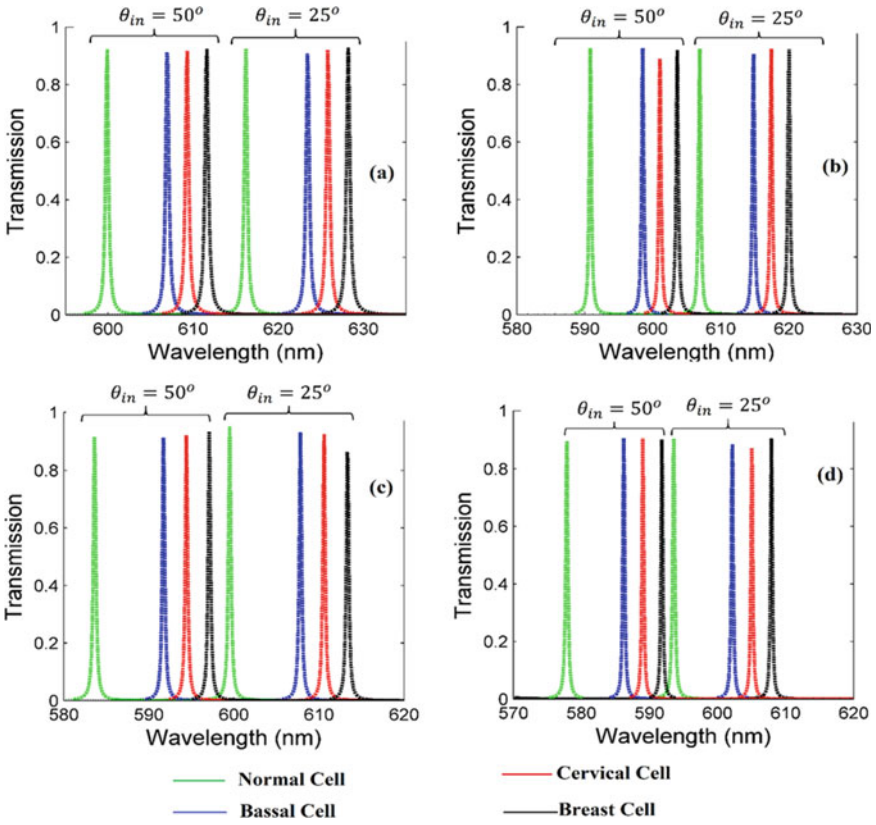

Fig. 8.7 Shift in the resonant modes for $\theta_{in} = 25°$ and 50° for **a** $d_D = 500$ nm, **b** $d_D = 600$ nm, **c** $d_D = 700$ nm, **d** $d_D = 800$ nm

is illustrated in Fig. 8.8a. By incrementing the L value, it is perceived that λ_{res} is moved to higher wavelength. On the other hand, with an increase in L, the intensity of the resonant mode goes on decreasing. As L increases, the effective thickness of the proposed design increases, which in turn escalate the geometrical path difference. Due to this reason, the wavelength is red-shifted. Based on this analysis, we chose monolayer of graphene ($L = 1$) as the optimized condition, where the most desirable characteristics are attained. Further, the effect of chemical potential (μ_c) across the graphene sheet can have a noteworthy effect on the device performance, which is examined in Fig. 8.8b. Here, it is perceived that at a constant L, the λ_{res} is red-shifted with rise in the chemical potential. With a variation in the chemical potential, the permittivity of the graphene sheet is changed, hence the red-shifting nature is observed in the λ_{res}.

In Fig. 8.9, the solid line and the dashed line indicate the transmission characteristics at $\mu_c = 0.3$eV and $\mu_c = 0.4$eV, respectively. From this figure, it is affirmed that by increasing the μ_c, the defect mode wavelength is moved to higher

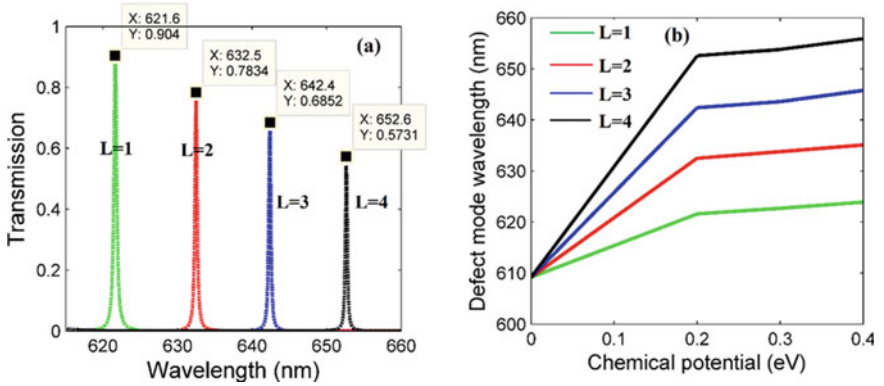

Fig. 8.8 **a** Transmittance as a function of L and **b** effect of chemical potential on the defect mode position

wavelength value for the normal as well as the cancer cells, so μ_c can greatly affect the sensing performance. As the defect modes are formed within the bandgap, there is possibility of absorption with different cells, and the same is analyzed in Fig. 8.10. As we change the cell type from the normal cells to the high refractive indexed cancer cells, the defect mode wavelength is red-shifted. Additionally, the absorption intensity increases for high indexed cancer cells.

Evaluation of sensitivity is outmost important to judge the performance It is explained as the ratio of shift in the defect mode wavelength with respect to different

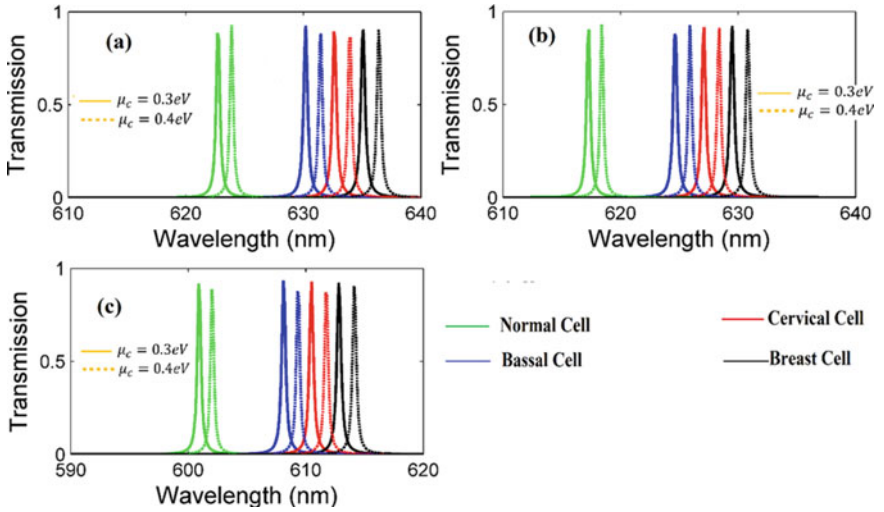

Fig. 8.9 Shifting the defect mode position w.r.t. μ_c at $d_D = 500$ nm for **a** $\theta_{\text{in}} = 0°$, **b** $\theta_{\text{in}} = 25°$, **c** $\theta_{\text{in}} = 50°$

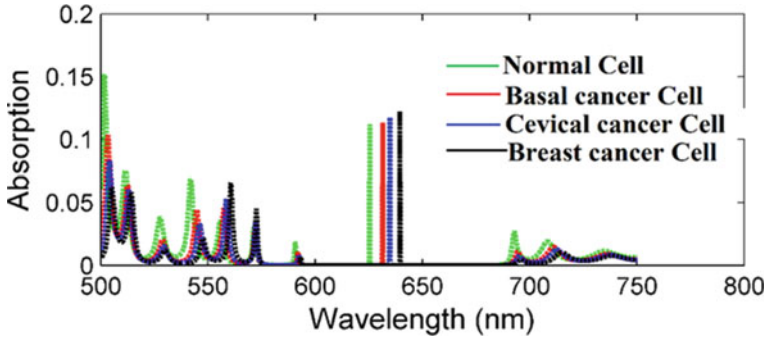

Fig. 8.10 Analysis of absorption spectra of different cells

cells under consideration. Sensitivity is written as [26],

$$S(\text{nm/RIU}) = \frac{\Delta\lambda_{\text{res}}}{\Delta n} \tag{8.17}$$

The sensitivity analysis at different incident angles is presented in Fig. 8.11. It is concluded that the sensitivity shows a declining trend with rise in the incidence angle and the sensitivity rises upon increasing the d_D. With the designed parameters $d_D =$ 800 nm and $\theta_{in} = 0°$, the maximum sensitivity of 290 nm/RIU is accomplished.

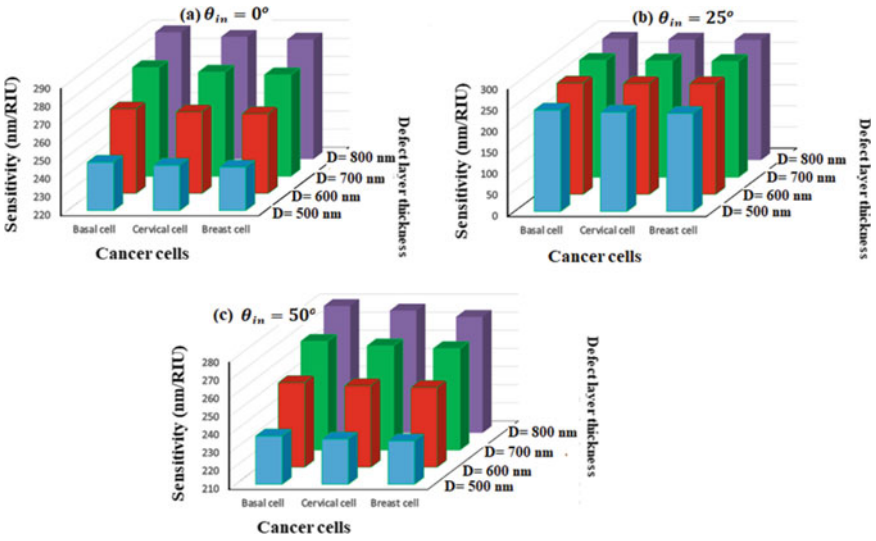

Fig. 8.11 Sensitivity analysis

Table 8.2 Measurement of sensor performance parameters

Cancerous cells	d_D (nm)	FoM (1/RIU)	QF	SNR	R (nm)
Basal	500	649.1	1640.5	19.4	0.121
Cervical		644.7	1646.3	25.7	0.113
Breast		642.1	1652.1	32.1	0.107
Basal	600	784.2	1808.2	23.5	0.103
Cervical		779.4	1815.8	31.1	0.096
Breast		776.4	1823.5	38.8	0.091
Basal	700	903.2	1960.6	27.0	0.090
Cervical		895.1	1969.6	35.8	0.084
Breast		890.3	1978.0	44.5	0.080
Basal	800	1074.0	2238.3	32.2	0.075
Cervical		1064.81	2255.7	42.5	0.070
Breast		1059.2	2270.7	52.9	0.066

Finally, other important performance parameters such as SNR, QF, resolution, and FoM are computed for different values of d_D at normal incidence and summarized in Table 8.2.

8.4 Conclusions

This chapter presents a novel graphene integrated photonic crystal configuration for the identification of numerous cancer cells. The layer thickness and incident angle can greatly control the spectral characteristics. The transmission spectrum is systematically scrutinized using TMM. The impact of chemical potential across the graphene sheet and the number of layers of graphene are studied on the sensing performance. The sensitivity is evaluated by assessing the defect mode wavelength shift between the normal cell and infected cancerous cells. A notable sensitivity of 290 nm/RIU, Q-factor of 2270.74, FoM of 1074.07 RIU^{-1}, SNR of 52.96, and resolution of 0.0668 have been accomplished with the designed structure. So, the authors are confident that the projected sensor can be the suitable candidate as cancer cells sensor.

References

1. Armstrong, E., Dwyer, C.O.: Artificial opal photonic crystals and inverse opal structures: fundamentals and applications from optics to energy storage. J. Mater. Chem. C **3**(24), 6109–6143 (2015)
2. Cucci, C., Tornari, V.: Photonic technologies for the safeguarding of cultural assets. In: Photonics for Safety and Security, pp. 21–45. World Scientific Press, Singapore (2014)
3. Shen, H., et al.: One-dimensional photonic crystals: fabrication, responsiveness and emerging applications in 3D construction. RSC Adv. **6**, 4505 (2016)
4. Yablonovitch, E.: Inhibited spontaneous emission in solid–state physics and electronics. Phys. Rev. Lett. **58**, 2059–2062 (1987)
5. John, S.: Strong localization of photons in certain in disordered dielectric superlattices. Phys. Rev. Lett. **58**, 2486–2489 (1987)
6. Ishizaki, K., Suzuki, K., Noda, S.: Fabrication of 3D photonic crystals toward arbitrary manipulation of photons in three dimensions. Photonics **3**(2), 36 (2016)
7. Panda, A., Pukhrambam, P.D.: Design and analysis of porous core photonic crystal fiber based ethylene glycol sensor operated at infrared wavelengths. J. Comput. Electron. **20**, 943–957 (2021)
8. Pang, L., Nakagawa, W., Fainman, Y.: Fabrication of two-dimensional photonic crystals with controlled defects by use of multiple exposures and direct write. Appl. Opt. **42**(27), 5450–5456 (2003)
9. Panda, A., Pukhrambam, P.D.: Photonic crystal biosensor for refractive index based cancerous cell detection. Opt. Fiber Technol. **54**, 102123 (2020)
10. Panda, A., Pukhrambam, P.D.: Analysis of GaN-based 2D photonic crystal sensor for real-time detection of alcohols. Braz. J. Phys. **51**, 481–492 (2021)
11. Baba, T., Mori, D., Inoshita, K., Kuroki, Y.: Light localizations in photonic crystal line defect waveguides. IEEE J. Sel. Top. Quant. Electron. **10**(3), 484–491 (2004)
12. Wellenzohn, M., et al.: Design of a photonic crystal defect waveguide biosensor operating in aqueous solutions at 1.34 μm, Proceedings **2**, 1026 (2018)
13. Moghaddam, M.K., Fleury, R.: Slow light engineering in resonant photonic crystal line-defect waveguides. Opt. Expr. **27**(18), 26229–26238 (2019)
14. Panda, A., Pukhrambam, P.D.: A theoretical proposal of high performance blood components biosensor based on defective 1D photonic crystal employing WS2, MoS2 and graphene. Opt. Quant. Electron. **53**(357) (2021)
15. Panda, A., Pukhrambam, P.D., Keiser, G.: Realization of sucrose sensor using 1D photonic crystal structure vis-à-vis band gap analysis. Microsyst. Technol. **27**, 833–842 (2021)
16. Panda, A., et al.: Research on SAD-PRD losses in semiconductor waveguide for application in photonic integrated circuits. Optik **154**, 748–754 (2018)
17. Panda, A., Pukhrambam, P.D.: Investigation of defect based 1D photonic crystal structure for real-time detection of waterborne bacteria. Phys. B Condens. Matter. **607**(3), 412854 (2021)
18. Aly, A.H., et al.: Theoretical study of hybrid multifunctional one-dimensional photonic crystal as a flexible blood sugar sensor. Phys. Scr. **95**(3), 035510 (2020)
19. Goyal, A., Suthar, B., Bhargava, A.: Biosensor application of one-dimensional photonic crystal for malaria diagnosis. Plasmonics **16**, 59–63 (2021)
20. Sharma, S., Kumar, A.: Design of a biosensor for the detection of dengue virus using 1D photonic crystals. Plasmonics (2021). https://doi.org/10.1007/s11468-021-01555-x
21. Abadla, M.M., Elsayed, H.A.: Detection and sensing of hemoglobin using one-dimensional binary photonic crystals comprising a defect layer. Appl. Opt. **59**(2), 418–424 (2020)
22. Algorri, J.F., et al.: Infiltrated photonic crystal fibers for sensing applications. Sensors **18**(12), 4263 (2018)
23. Panda, A., Pukhrambam, P.D.: Design and analysis of 1D photonic crystal doped with magnetized cold plasma defect for application of single/multi-channel tunable narrowband filter. Phys. Scr. **97**, 065507 (2022). https://doi.org/10.1088/1402-4896/ac6f92

24. Aly, A.H., Mohamed, D., Mohaseb, M.A., Abd El-Gawaad, N.S., Trabelsi, Y.: Biophotonic sensor for the detection of creatinine concentration in blood serum based on 1D photonic crystal, RSC Adv. **10**, 31765–31772 (2020)s
25. Panda, A., Vigneswaran, D., Pukhrambam, P.D., Ayyanar, N., Nguyen, T.K.: Design and performance analysis of reconfigurable 1D photonic crystal biosensor employing Ge2Sb2Te5 (GST) for detection of women reproductive hormones. IEEE Trans. NanoBiosci. 21(1), 21–28 (2022)
26. Panda, A., Pukhrambam, P.D., Wu, F., Belhadj, W.: Graphene-based 1D defective photonic crystal biosensor for real-time detection of cancer cells. Eur. Phys. J. Plus. **136**, 809 (2021)
27. Falkovsky, L.A., Pershoguba S.S.: Optical far-infrared properties of a graphene mono layer and multilayer. Phys. Rev. B **76**(15) (2007). Art. no. 153410
28. Mak, K.F., Shan, J., Heinz, T.F.: Electronic structure of few-layer graphene: experimental demonstration of strong dependence on stacking sequence. Phys. Rev. Lett. **104**, 176404 (2010)
29. Geim, A.K.: Graphene: status and prospects. Science **324**, 1530–1534 (2009)
30. Novoselov, K.S.: The rise of graphene. Nat. Mater. **6**, 183–191 (2007)
31. Bonaccorso, F., Sun, Z., Hasan, T., Ferrari, A.C.: Graphene photonics and optoelectronics. Nat. Photonics **4**, 611–622 (2010)
32. Stauber, T., Peres, N.M.R., Geim, A.K.: Optical conductivity of graphene in the visible region of the spectrum. Phys. Rev. B **78**(8) (2008). Art. no. 085432
33. Schedin, F., Geim, A., Morozov, S., Hill, E., Blake, P., Katsnelson, M., Novoselov, K.: Detection of individual gas molecules adsorbed on graphene. Nat. Mater. **6**, 652 (2007)
34. Pop, E., et al.: Thermal properties of graphene: fundamentals and applications. MRS Bull. **37**, 1273–1281 (2012)
35. Rahman, M. R., et al.: Electrical and chemical properties of graphene over composite materials: a technical review. Mat. Sci. Res. India **16**(2) (2019)
36. Liao, G., et al.: Preparation properties, and applications of graphene-based hydrogels. Front. Chem. **6**, 450 (2018)
37. Nouman, W.M., Abd El-Ghany, S.E.S., Sallam, S.M., et al.: Biophotonic sensor for rapid detection of brain lesions using 1D photonic crystal. Opt. Quant. Electron. **52**, 287 (2020)
38. Zaky, Z.A., Ahmed, A.M., Shalaby, A.S., Aly, A.H.: Refractive index gas sensor based on the Tamm state in a one-dimensional photonic crystal: Theoretical optimization. Sci. Rep. **10**, Art. no. 9736 (2020)
39. Shi, X., Zhao, Z.S., Han, Z.H.: Highly sensitive and selective gas sensing using the defect mode of a compact terahertz photonic crystal cavity. Sens. Actuators **274**, 188–193 (2018)
40. Ahmed, A.M., Mehaney, A.: Ultra-high sensitive 1D porous silicon photonic crystal sensor based on the coupling of Tamm/Fano resonances in the mid-infrared region. Sci Rep **9**, 6973 (2019)
41. Aly, A.H., et al.: Biophotonic sensor for the detection of creatinine concentration in blood serum based on 1D photonic crystal. RSC Adv. **10**, 31765–31772 (2020)
42. Abadla, M.M., Elsayed, H.A.: Detection and sensing of hemoglobin using one-dimensional binary photonic crystals comprising a defect layer. Appl. Opt. **59**(2), 418–424 (2020)
43. Bouzidi, A., Bria, D., Falyouni, F., Akjouj, A., Lévêque, G., Azizi, M., Berkhli, H.: A biosensor based on one dimensional photonic crystal for monitoring blood glycemia. J. Mater. Environ. Sci. **8**(11), 3892–3896 (2017)
44. Elsayed, H.A., Mehaney, A.: Theoretical verification of photonic crystals sensor for biodiesel detection and sensing. Phys. Scr. **95**, 085507 (2020)
45. Fu, J., Chen, W., Lv, B.: Tunable defect mode realized by graphene-based photonic crystals. Phys. Lett. A **380**, 1793–1798 (2016)
46. Fan, H.M.: Tunable plasmonic band gap and defect mode in one dimensional photonic crystal covered with graphene. J. Opt. **16** (2014). Art. no. 125005
47. Abd El-Aziz, O.A., Elsayed, H.A., Sayed, M.I.: One-dimensional defective photonic crystals for the sensing and detection of protein. Appl. Opt. **58**(30), 8309–8315 (2019)
48. Katz, R., Edelson, M.: The Cancer-Fighting Kitchen: Nourishing, Big-Flavor Recipes for Cancer. Ten Speed Press, Crown Publishing Group, New York, USA (2009)

49. Bray, F., Ferlay, J., Soerjomataram, I., Siegel, R.L., Torre, L.A., Jemal, A.: Global cancer statistics 2018: GLOBOCAN estimates of incidence and mortality worldwide for 36 cancers in 185 countries. CA Cancer J. Clin. **68**, 394–424 (2018)
50. Yaroslavsky, A.N., et al.: High-contrast mapping of basal cell carcinomas. Opt. Lett. **37**(4), 644–646 (2012)
51. Bijalwan, A., Singh, B.K., Rastogi, V.: Analysis of one-dimensional photonic crystal based sensor for detection of blood plasma and cancer cells. Optik **226**(1), 165994 (2021)
52. Aly, A.H., Zaky, Z.A.: Ultra-sensitive photonic crystal cancer cells sensor with a high quality factor. Cryogenics **104**, 102991 (2019)
53. Ramanujam, N.R., Amiri, I., Taya, S.A., Olyaee, S., Udaiyakumar, R., Pandian, A.P.: Enhanced sensitivity of cancer cell using one dimensional nano composite material coated photonic crystal. Microsyst. Technol. **25**, 189–196 (2019)
54. Panda, A., Devi, P.P.: Photonic crystal biosensor for refractive index based cancerous cell detection. Opt. Fiber Technol. **54**, 102123 (2020)
55. Ayyanar, N., Raja, G.T., Sharma, M., Kumar, D.S.: Photonic crystal fiber-based refractive index sensor for early detection of cancer. IEEE Sens. J. **18**, 7093–7099 (2018)
56. Sani, M.H., Khosroabadi, S.: A novel design and analysis of high-sensitivity biosensor based on nano-cavity for detection of blood component, diabetes, cancer and glucose concentration. IEEE Sens. J. **20**(13), 7161–7168 (2020)
57. Jabin, M.A., et al.: Surface plasmon resonance based titanium coated biosensor for cancer cell detection. IEEE Photonics J. **11**(4), 1–10 (2019)
58. https://refractiveindex.info/?shelf=main&book=ZnSe&page=Marple
59. https://refractiveindex.info/?shelf=main&book=MgF2&page=Dodge-o
60. Kumar, A., Singh, P., Thapa, K.B.: Study of super absorption properties of 1D graphene and dielectric photonic crystal for novel applications. Opt. Quant. Electron. **52** (2020)
61. Ghasemi, F., Entezar, S.R., Razi, S.: Terahertz tunable photonic crystal optical filter containing graphene and nonlinear electro-optic polymer. Laser Phys. **29**, 056201 (2019)
62. Liang X.J., et al.: Determination of refractive index for single living cell using integrated biochip. In: Solid-State Sensors, Actuators and Microsystems, 2005. Digest of Technical Papers. TRANSDUCERS'05., vol. 2, pp. 1712–1715. IEEE (2005)
63. Sharan, P., Bharadwaj, S. M., Gudagunti, F.D., Deshmukh, P.: Design and modelling of photonic sensor for cancer cell detection. In: Impact of E-Technology on US (IMPETUS), IEEE International Conference on the, pp. 20–24. IEEE (2014)